AIChE

Modeling Continuous Electropermutation with Effects of Water Dissociation Included

Carl-Ola Danielsson and Anders Dahlkild
Dept. of Mechanics, School of Engineering Science, Royal Institute of Technology, Stockholm, SE-100 44, Sweden

Anna Velin
Vattenfall Research and Development AB, Stockholm, SE-162 87, Sweden

Mårten Behm
Applied Electrochemistry, Dept. of Chemical Engineering and Technology, School of Chemical Science and Engineering, Royal Institute of Technology, Stockholm, SE-100 44, Sweden

DOI 10.1002/aic.12139
Published online January 22, 2010 in Wiley Online Library (wileyonlinelibrary.com).

The repeating unit consisting of a cell pair of one concentrate and one feed compartment of an electropermutation stack is modeled. Both the feed and the concentrate compartments are filled with an ion-exchange textile material. Enhanced water dissociation taking place at the surface of the membrane is included in the model as a hetrogeneous surface reaction. Results from simulations of nitrate removal for drinking water production are presented and comparisons with previous experimental results are made. The influence of both conductive and inert textile spacers on the process is investigated via simulations. © 2010 American Institute of Chemical Engineers *AIChE J,* 56: 2455–2467, 2010
Keywords: ion exchange, mathematical modeling, membrane separations, electrochemistry, simulation, process

Introduction

Ion exchange and electrodialysis are two widely used process alternatives for separation of ionic impurities from water. The advantage of ion exchange is that it is capable of treating solutions with very low levels of pollutants.[1] However, ion exchange is not a continuous process. Electrodialysis on the other hand is a continuous process but is not suitable for treatment of solutions with very low conductivity. In electrodeionization (EDI),[2,3] both these processes are combined into a continuous process, which is capable of treating solutions of very low conductivity. EDI is mainly used for production of ultrapure water. The main application for EDI is production of ultrapure water that is used in the power, microelectronics, and pharmaceutical industry. In these applications, all ions in the water need to be removed. Hence, an ion exchange bed that contains both cation and anion exchange material is used.

Continuous electropermutation[4–7] is a process, which is similar to EDI in that it combines conventional ion-exchange with an electromembrane process. Instead of removing all ions either the anions or the cations are selectively replaced by other more desirable ions. Thus, the ion exchange bed should consist of either anion or cation exchange material. An application where electropermutation is an interesting process alternative is the removal of nitrate in drinking water production. Depending on the quality of the raw water one might like to selectively replace the nitrate ions. The principle for nitrate removal using continuous electropermutation is presented in Figure 1. The water to be treated is passed

Correspondence concerning this article should be addressed to C.-O. Danielsson at carl.ola.d@gmail.com.

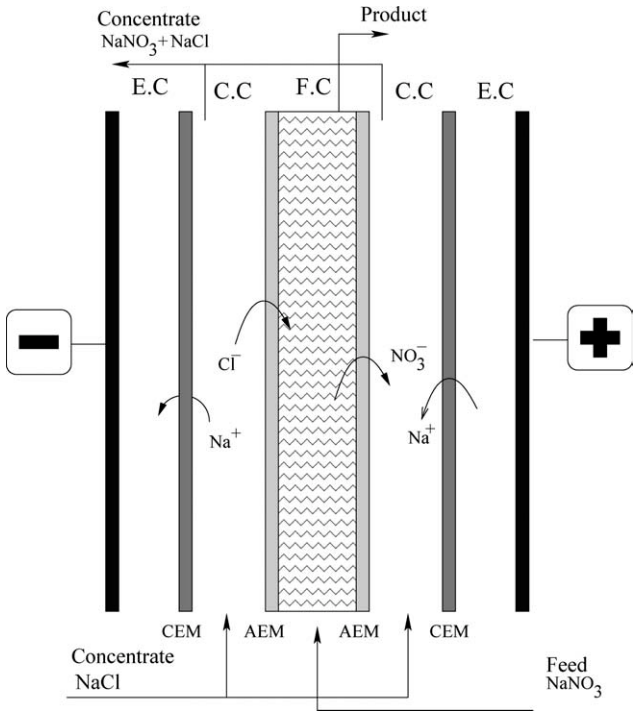

Figure 1. A schematic over the principles behind continuous electropermutation for nitrate removal.

The water to be treated is passed through the feed compartment (F.C), which is separated from the concentrate compartments by anion permeable membranes on each side. Under the influence of an applied electric field, the nitrate ions in the F.C are replaced by chloride ions from the C.C.

through the feed compartment (FC), which is delimited by two anion permeable membranes. Under the influence of an applied electric field, the anions in the system migrates toward the anode. The anions present in the feed water migrate over the membrane into the Concentrate Compartment (CC) located on the anode side of the FC. Electroneutrality is maintained by other anions entering from the CC on the cathode side of the FC. This way it is possible to replace the anions initially present in the feed by anions from the concentrate solution, whereas the cations are preserved. In the schematic presented in Figure 1, the nitrate ions migrate out from the FC over the right hand side membrane at the same time as chloride ions enter the FC over the left hand side membrane. The solution in the concentrate compartment in this example is a concentrated sodium chloride solution. Depending on the quality of the feed water the concentrate solution can be tailored, e.g., to adjust the pH by replacing the nitrate ions partially with hydroxide.

In two previous papers,[6,7] the removal of nitrate by continuous electropermutation using ion exchange textile as conductive spacer was studied both experimentally and theoretically. From the experimental investigation, it was concluded that a conductive spacer is needed, in the FC, for the electropermutation process to be operated at reasonable current densities. Without a conductive spacer, the limiting current density was very low and increasing the potential further led to intense water dissociation. Incorporation of an ion-exchange textile as a conductive spacer in the FC greatly increased the efficiency of the process. It was concluded that the electropermuation process is an interesting process alternative for production of drinking water. However, also with the ion-exchange textile incorporated as a conductive spacer, it was noted that water dissociation was starting to become important at an average current density of 25 A/m^2. The effect of water dissociation as a parasitic reaction was not considered in the electropermutation model presented in Ref. 6. To include this additional phenomenon, a model of water dissociation, treated as a potential-dependent heterogeneous reaction, was developed.[8] An important task of this work is to test that model in a simulation of the entire electropermutation process, and to compare with the experimental results of Ref. 7. Finally, this improved electropermutation model will be used to study how the incorporation of the textile influences the dissociation of water, and the overall behavior of the process.

Problem Formulation

In a previous paper, a steady state model of the FC, filled with an ion-exchange textile as a conductive spacer, together with adjacent ion-exchange membranes in an electropermutation cell was presented.[6] In this article that model will be extended to include also the effect of water dissociation. Hence, the homogeneous reaction

$$H_2O \underset{k_b}{\overset{k_f}{\rightleftarrows}} OH^- + H^+ \tag{1}$$

is considered. It is known that enhanced water dissociation can occur at the surface of the anion exchange membrane. The heterogeneous model used to incorporate this enhanced water dissociation was presented in a separate paper.[8] The repeating unit in an electropermutation stack consists of one CC and one FC. A sketch of the domain included in the model is presented in Figure 2. The CC is split into two halves, subdomains I and

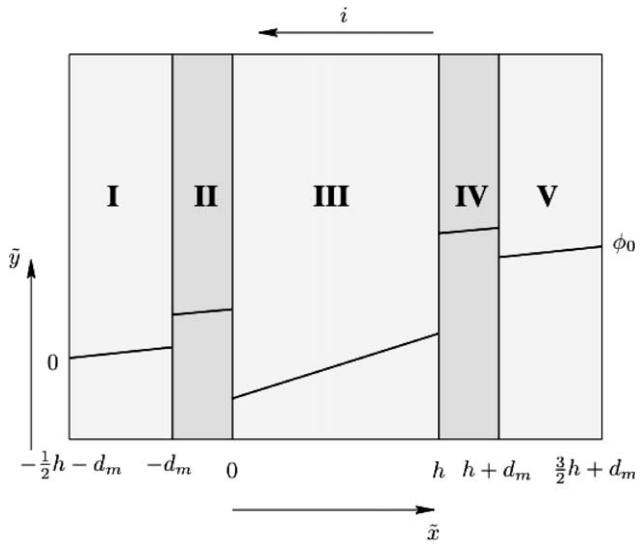

Figure 2. A schematic of the domain included in the model.

I: Half of the adjacent CC II: Anion permeable membrane. III: FC IV: Anion permeable membrane. V: Half of the adjacent CC. The solid line is a schematic of the potential through the cell.

V, these are located on opposite sides of the central FC, subdomain III. Anion permeable membranes, subdomains II and IV, separate the concentrate and FC. Periodic boundary conditions are applied at the center of the concentrate compartment, i.e., between subdomain I and V, except for the potential.

Mass balance equations are formulated for the following species NO_3^-, Cl^-, Na^+, OH^-, and H^+, which will be denoted as Species 1–5, respectively. Thus, a whole elementary cell is now included in the model. Furthermore, the boundary layers next to the membranes are resolved instead of using the simplified Nernst layer model.

The feed and concentrate compartments are filled with an ion-conductive textile. Besides providing a good conductivity in the FC, this textile material will help to accomplish a good mixing of the solution as well as providing mechanical support to the membranes. The FC is delimited by two anion permeable membranes, which are assumed to be ideally selective. The coordinate intervals of the five subdomains of the model domain, shown in Figure 2, are

I. Half of the adjacent concentrate compartment

$$-\frac{h}{2}-d^{\mathrm{m}} \le \tilde{x} \le -d^{\mathrm{m}}$$

II. Anion-permeable membrane

$$-d^{\mathrm{m}} \le \tilde{x} \le 0$$

III. Feed compartment

$$0 \le \tilde{x} \le h$$

IV. Anion-permeable membrane

$$h \le \tilde{x} \le h + d^{\mathrm{m}}$$

V. Half of the adjacent concentrate compartment

$$h + d^{\mathrm{m}} \le \tilde{x} \le \frac{3}{2}h + d^{\mathrm{m}}$$

Momentum Balance

In the previous model,[6] the flow through the textile-filled FC was modeled with Darcy's law, which in the case of a unidirectional pressure gradient and a homogeneous textile gave a plug flow through the FC

$$\tilde{\mathbf{j}} = -\frac{K}{\mu}\frac{\partial P}{\partial \tilde{y}}\mathbf{e}_y \tag{2}$$

where $\tilde{\mathbf{j}}$ is the velocity vector, K is the permeability of the textile, μ the dynamic viscosity and P is the pressure. The effect of velocity boundary layers, satisfying the no-slip condition at the membrane walls, on mass transport next to the membranes was modeled by a stagnant Nernst layer. Because of the rapid reaction kinetics of the introduced homogeneous water dissociation/recombination reaction, the simplified Nernst layer model will not account for the nonequilibrium reaction layer close to the membrane. To include this reaction layer, the momentum boundary layers are also resolved in this article. This is done by adding the Brinkman extension to Darcy's law.[9] The flow field is obtained by solving the following equation:

$$\frac{\partial^2 \tilde{j}_y}{\partial \tilde{\xi}^2} - \frac{(1-\varepsilon)}{K}\tilde{j}_y - \frac{(1-\varepsilon)}{\mu}\frac{\partial P}{\partial \tilde{y}} = 0 \tag{3}$$

with the boundary conditions

$$\tilde{j}_y(\xi = 0) = 0, \quad \frac{\partial \tilde{j}_y}{\partial \tilde{\xi}}(\xi = \infty) = 0, \tag{4}$$

where ξ is the coordinate in the wall normal direction. ε in the equation above is the volume fraction of the fibers.

The permeability is taken to be a function of the porosity and the fiber diameter.[10] For a fibrous medium, the following expression can be found in the literature[11,12]:

$$K = \frac{3d_{\mathrm{f}}^2}{20\varepsilon}[-\ln(\varepsilon) - 0.931]. \tag{5}$$

The pressure gradient is assumed to be constant. Thus, the velocity profile is given by

$$\tilde{j}_y(\xi) = j_0(1 - \exp(-\sqrt{(1-\varepsilon)K^{-1}}\xi)), \tag{6}$$

where j_0 is the "plug flow" velocity in the bulk of the textile bed. The nondimensional velocity is obtained by scaling with j_0,

$$\mathbf{j} = \frac{\tilde{\mathbf{j}}}{j_0}. \tag{7}$$

Mass Balance Equations

Feed and Concentrate compartments

The textile-filled feed and concentrate compartments, i.e., subdomains I,III, and V, are treated as two-phase porous media with a liquid and a fibre phase. A more in depth derivation and analysis of the model equations, for a case without water dissociation, was presented in our previous paper[6] in which it was shown that the liquid phase and the fiber phase can be considered to be in ion-exchange equilibrium with each other. Thus, it is sufficient to solve one mass balance equation for each species. Furthermore, it was shown that the streamwise flux was totally dominated by convection in the liqud phase. The general mass balance equation to solve for each species is given by

$$\frac{\partial \tilde{N}_{i,y}}{\partial \tilde{y}} + \frac{\partial(\tilde{N}_{i,x} + \bar{\tilde{N}}_{i,x})}{\partial \tilde{x}} = \tilde{S}_i \tag{8}$$

where the bar is over the flux in the fibre phase. In the expression, the reaction term, $\tilde{S}_i$, vanishes for the species $i = 1 - 3$. For species 4 and 5 the reaction term is given by

$$\tilde{S}_i = (1-\varepsilon)k_{\mathrm{b}}K_{\mathrm{w}}\left(1 - \frac{\tilde{c}_4\tilde{c}_5}{K_{\mathrm{w}}}\right), \tag{9}$$

where k_{b} and $K_{\mathrm{w}} = \frac{k_{\mathrm{f}}\tilde{c}_{H_2O}}{k_{\mathrm{b}}}$ are taken to be constants.

For the nondimensional form of the governing Eq. 8, the following variables are introduced

$$x=\frac{\tilde{x}}{h},\quad y=\frac{\tilde{y}}{L},\quad c_i=\frac{\tilde{c}_i}{c_0},\quad \bar{c}_i=\frac{\bar{\tilde{c}}_i}{w},\quad \phi=\frac{\tilde{\phi}}{\phi_0},\quad \bar{\phi}=\frac{\bar{\tilde{\phi}}}{\phi_0}, \tag{10}$$

where the tildes are over the dimensional variables. h and L are the width and length of the FC, respectively. c_0 is a typical concentration at the inlet to the FC and w is the concentration of fixed charges in the fibre phase. ϕ_0 is the total voltage drop over the repeating unit e.g., from the middle of one CC to middle of the next.

In this article, the volume-averaged flux densities are all scaled by $\frac{D_0 c_0}{h}$. The nondimensional convective vertical flux is then given by

$$N_{i,y}=\frac{L}{h}\hat{P}e j_y c_i \tag{11}$$

where the diffusive and migration fluxes have been neglected in both phases. The Peclet number, $\hat{P}e=\frac{h}{L}\frac{j_0 h}{D_0}$, measures the ratio of the vertical convective and horizontal diffusive flux densities scaled with the aspect ratio to account for the narrow shape of the channel. The nondimensional horizontal fluxes are expressed as

$$N_{i,x}=-(j_y\theta\hat{P}e+(1-\varepsilon)^{3/2}D_i)\frac{\partial c_i}{\partial x}-z_i\mathcal{V}(1-\varepsilon)^{3/2}D_i c_i\frac{\partial\phi}{\partial x} \tag{12}$$

in the liquid phase, and

$$\bar{N}_{i,x}=-0.15Z\varepsilon^{3/2}D_i\left(\frac{\partial\bar{c}_i}{\partial x}-z_i\mathcal{V}\bar{c}_i\frac{\partial\bar{\phi}}{\partial x}\right) \tag{13}$$

in the fibrous phase. The fluxes in both phases have terms representing molecular diffusion and migration, where the nondimensional diffusion coefficients are defined according to;

$$D_i=\frac{\tilde{D}_i}{D_0},\ \bar{D}_i=\frac{\bar{\tilde{D}}_i}{D_0}, \tag{14}$$

and where it was assumed that the diffusion coefficients in the fibre phase are related to those in water as[1,6]:

$$\bar{D}_i=0.15D_i. \tag{15}$$

The aforementioned flux expressions were derived under the assumption that the two phases are in a parallel arrangement with each other. Effective diffusion coefficients, given by a Bruggeman relation, have been used in both phases

$$D_{i,\text{eff}}=(1-\varepsilon)^{3/2}D_i\quad\text{and}\quad\bar{D}_{i,\text{eff}}=\varepsilon^{3/2}\bar{D}_i. \tag{16}$$

The use of the effective diffusion coefficients compensate to some extent for the assumption of a parallel arrangement of the phases.

The liquid phase also has a contribution from the mechanical dispersion. The correlation used for the dimensional transverse dispersion coefficient is given by,[10,13]

$$D_T=\lambda\tilde{j}_y d_f \tag{17}$$

where λ is an empirical parameter and d_f is the fibre diameter. The only difference in the ionic transport model compared to the derivation presented in our previous paper[6] is that the molecular diffusion in the liquid phase is not neglected. The reason for this is that close to the membranes the mechanical dispersion will vanish and hence molecular diffusion and migration will dominate in this region.

The flow velocity, j_y, is given by,

$$\begin{aligned}
&j_y=1-\exp(\Lambda(x+\Theta))\quad\text{for}\quad-\Theta-0.5\le x\le-\Theta\\
&j_y=1-\exp(-\Lambda x)\quad\text{for}\quad 0\le x\le 0.5\\
&j_y=1-\exp(-\Lambda(1-x))\quad\text{for}\quad 0.5\le x\le 1\\
&j_y=1-\exp(-\Lambda(x-1-\Theta))\quad\text{for}\quad 1+\Theta\le x\le\Theta+1.5
\end{aligned} \tag{18}$$

where $\Theta=\frac{d_m}{h}$ is the ratio between the membrane thickness to the width of the FC. $\Lambda=\sqrt{\frac{(1-\epsilon)}{K}}h$ is the ratio between a typical length scale of the porous medium and the FC width, which determines the shape of the velocity profile in the feed and concentrate compartments.

The following nondimensional parameters were also introduced earlier

$$\hat{P}e=\frac{h}{L}\frac{j_0 h}{D_0},\ \theta=\frac{\lambda d_f L}{h^2},\ \mathcal{V}=\frac{F\phi_0}{\mathrm{RT}}. \tag{19}$$

θ is an inverse Peclet number for the diffusion due to mechanical dispersion, and $\mathcal{V}$ is the nondimensional cell voltage.

Inserting the expressions for the reaction term and the volume averaged fluxes, i.e. Eqs 9, 12, and 13, in the mass balance expression, Eq. 8 gives,

$$\begin{aligned}
j_y\frac{\partial c_i}{\partial y}=&\left(\theta j_y+(1-\varepsilon)^{3/2}\frac{D_i}{\hat{P}e}\right)\frac{\partial^2 c_i}{\partial x^2}\\
&+z_i\frac{\mathcal{V}}{\hat{P}e}(1-\varepsilon)^{3/2}D_i\frac{\partial}{\partial x}\left(c_i\frac{\partial\phi}{\partial x}\right)+\frac{0.15\varepsilon^{3/2}}{\hat{P}e}D_i\frac{\partial^2\bar{c}_i}{\partial x^2}\\
&+z_i 0.15\frac{\mathcal{V}}{\hat{P}e}\varepsilon^{3/2}D_i\frac{\partial}{\partial x}\left(\bar{c}_i\frac{\partial\bar{\phi}}{\partial x}\right)+\kappa_i(1-c_4c_5).
\end{aligned} \tag{20}$$

The ion-exchange fibers are assumed to be in equilibrium with the solution, which gives,

$$\begin{aligned}
\bar{c}_2&=\alpha_1^2\frac{\bar{c}_1 c_2}{c_1}\\
\bar{c}_4&=\alpha_1^4 Z\frac{\bar{c}_1 c_4}{c_1}.
\end{aligned} \tag{21}$$

Furthermore, the potential gradient in the two phases are related through

$$\frac{\partial\bar{\phi}}{\partial x}=\frac{\partial\phi}{\partial x}+\frac{1}{\mathcal{V}}\frac{\partial}{\partial x}\ln\left[\frac{Z}{c_1+\alpha_1^2c_2+\alpha_1^4c_4}\right]. \tag{22}$$

The additional nondimensional parameters introduced earlier are defined according to:

$$\kappa = \frac{(1-\varepsilon)LK_{\mathrm{w}}k_{\mathrm{b}}}{c_0 j_0},\ Z = \frac{w}{c_0} \tag{23}$$

where κ is the nondimensional reaction rate constant and Z is the ratio between the capacity of the fibre phase and the concentration in the feed. In Ref. 6 it was shown that the ratio

$$\chi = \frac{\mathcal{V}}{\hat{P}e} \tag{24}$$

measuring the relative importance of the horizontal flux due to migration to the convective vertical flux, was critical when describing different features of the process. Thus, in the simulations χ rather than $\mathcal{V}$, was used as an independent nondimensional parameter.

Membranes

In the membranes only the anionic species (i = 1,2,4) are present. Contribution to the flux through the membranes by convection is neglected, thus, using the same scaling of the fluxes through the membranes as in the feed and concentrate compartment gives

$$N_{i,x}^{\mathrm{m}} = -C^{\mathrm{m}}\left(D_i^{\mathrm{m}}\frac{\partial c_i^{\mathrm{m}}}{\partial x} - z_i\mathcal{V}D_i^{\mathrm{m}}c_i^{\mathrm{m}}\frac{\partial \phi^{\mathrm{m}}}{\partial x}\right) \quad \text{for} \quad i = 1,2,4. \tag{25}$$

In the aforementioned expression, the following new dimensionless variables and parameters were introduced;

$$c_i^{\mathrm{m}} = \frac{\tilde{c}_i^{\mathrm{m}}}{c_0^{\mathrm{m}}},\quad \phi^{\mathrm{m}} = \frac{\tilde{\phi}^{\mathrm{m}}}{\phi_0},\quad D_i^{\mathrm{m}} = \frac{\tilde{D}_i^{\mathrm{m}}}{D_0},\quad C^{\mathrm{m}} = \frac{c_0^{\mathrm{m}}}{c_0}, \tag{26}$$

where c_0^{m} is the concentration scale in the membrane, which was taken to be equal to the ion-exchange capacity of the membrane.

The nondimensional form of the mass balance equations in the membranes is given by:

$$-\frac{\partial^2 c_i^{\mathrm{m}}}{\partial x^2} + \mathcal{V}\frac{\partial}{\partial x}\left(c_i^{\mathrm{m}}\frac{\partial \phi^{\mathrm{m}}}{\partial x}\right) = 0 \quad \text{for} \quad i = 1,2,4. \tag{27}$$

Electroneutrality conditions

Electroneutrality is assumed in all regions of the model and the nondimensional form of this constraint is given by:

$$\begin{aligned} &c_1^{\mathrm{m}} + c_2^{\mathrm{m}} + c_4^{\mathrm{m}} = 1 \quad \text{in subdomains II and VI}\\ &c_1 + c_2 + c_4 = c_3 + c_5 \quad \text{in the liquid phase in subdomain I, III, V}\\ &\bar{c}_1 + \bar{c}_2 + \bar{c}_4 = 1 \quad \text{in the fiber phase in subdomain I, III, V.} \end{aligned} \tag{28}$$

Boundary conditions

The composition of the feed water gives the boundary conditions at the inlet boundary

$$c_i|_{y=0} = c_{i0} \quad \text{for} \quad i = 1-5 \tag{29}$$

Periodic boundary conditions are applied for all concentrations at the center of the concentrate compartment,

$$c_i|_{x=-0.5-\Theta} = c_i|_{x=1.5+\Theta}. \tag{30}$$

The potential difference over the cell is prescribed leading to the following boundary conditions:

$$\phi|_{x=-0.5-\Theta} = 0 \quad \text{left boundary} \tag{31}$$

$$\phi|_{x=1.5+\Theta} = 1 \quad \text{right boundary.} \tag{32}$$

Internal Boundary Conditions. At the internal boundaries, all electrochemical potentials as well as all flux densities are continuous except for H^+ and OH^-. The locally enhanced water dissociation at the membrane interfaces is modeled by a surface reaction. Therefore, the flux densities of protons and hydroxide ions are allowed to be discontinuous at the membrane interfaces. The model for this surface reaction was presented in a previous paper.[8] The continuity of electrochemical potential gives rise to the following internal boundary conditions for the potential,

$$\phi = \phi^{\mathrm{m}} + \frac{1}{\mathcal{V}}\ln\left[\frac{c_1 + c_2 + c_4}{C^{\mathrm{m}}}\right] \tag{33}$$

at the internal boundaries between subdomains.

Internal boundary conditions for the concentrations are also obtained from the continuity of the electrochemical potential according to,

$$\begin{aligned} c_2^{\mathrm{m}} &= \alpha_1^{\mathrm{m}2}\frac{c_1^{\mathrm{m}}c_2}{c_1} \quad \text{and}\\ c_4^{\mathrm{m}} &= \alpha_1^{\mathrm{m}4}\frac{c_1^{\mathrm{m}}c_4}{c_1}. \end{aligned} \tag{34}$$

Continuity of the fluxes of species NO_3^- and Cl^- over all subdomain boundaries gives,

$$N_{i,x} + \bar{N}_{i,x} = N_{i,x}^{\mathrm{m}} \quad \text{for} \quad i = 1,2. \tag{35}$$

The membranes are assumed to be ideally selective, which leads to a zero flux condition for sodium at the membrane surfaces,

$$N_{3,x} = N_{3,x}^{\mathrm{m}} = 0, \tag{36}$$

at all internal bounaries.

At the boundary between subdomains II and III, i.e., x = 0, and between subdomains IV and V, i.e., $x = 1+\Theta$ the total ionic concentration next to the membrane will increase and thus the enhanced water dissociation is neglected at these boundaries. Continuity of fluxes at these interfaces gives

$$N_{4,x}^{\mathrm{m}} = N_{4,x} + \bar{N}_{4,x} \tag{37}$$

and the ideal selectivity of the membranes gives a zero flux of the cations over the membrane surface, i.e.,

$$N_{5,x} = N_{5,x}^{\mathrm{m}} = 0. \tag{38}$$

At the boundary between subdomains I and II, i.e., $x = -\Theta$, and between sub domains III and IV, i.e., $x = 1$, the fluxes of OH^- and H^+ are not continuous due to the enhanced water dissociation, which is modeled by a heterogeneous surface reaction. Thus, the flux condition for OH^- and H^+ is given by:

$$N_{4,x} + \bar{N}_{4,x} + \mathcal{R} = N_{4,x}^{\mathrm{m}} \tag{39}$$

and

$$N_{5,x} + \mathcal{R} = 0, \tag{40}$$

where $\mathcal{R}$ is the heterogeneous surface reaction rate. The model for $\mathcal{R}$ was presented in a previous paper,[8]

$$\mathcal{R} = \Upsilon\left(\frac{C^{\mathrm{m}}}{c_1 + c_2 + c_4}\right)^{\alpha}\left(1 - \frac{c_4 c_5}{C^{\mathrm{w}}}\right), \tag{41}$$

where α is an empirical parameter. The parameter Υ is defined as

$$\Upsilon = \frac{k_{\mathrm{b}}^0 h K_{\mathrm{w}}}{c_0 D_0}, \tag{42}$$

where k_{b}^0 is the reaction rate constant per unit area, at zero potential difference over the reaction layer. In the aforementioned expression, the surface reaction rate was scaled in the same way as the fluxes, i.e., with $\frac{D_0 c_0}{h}$.

Results and Discussion

The model equations were implemented in the commercial finite element package Comsol Multiphysics™. The parabolic nature of the equations allowed them to be solved using a 1-D transient solver instead of a 2-D steady state. One advantage of this is that the adaptive time stepping ensured that sufficient numerical resolution was obtained in the streamwise direction. Furthermore, a very fine grid could be used because the grid resolved only one space dimension. A grid independence test was conducted to ensure that the mesh used in the simulations was sufficiently fine.

Comparison with experiments

Simulations were performed to compare the model predictions with the previously presented experimental results.[7] In Figures 3 and 4, the results from two different experiments are presented together with results obtained from simulations of these experiments. Figure 3 gives the variation of the nitrate concentration in the product water with the applied current density. The asterisk symbols show results from the experiment where the FC was filled with a nonconductive net-type spacer, case E in Ref. 7. It was found that a significant amount of nitrate was removed by Donnan dialysis, i.e., without the help of an external electric field, whereas applying an electric field did not lead to a great improvement of the nitrate separation. The limiting current density was low and increasing the current density above this is accomplished by dissociation of water. A sudden drop of the product pH was obtained when the average current density was increased from 5 to 10 A/m^2, which indicates that water dissociation has started to occur in the FC. Increasing the current density even further only gave a small increase in the flux of nitrate out from the feed compartment. Hence, the nitrate level in the product remained more or less constant as the applied current density was increased.

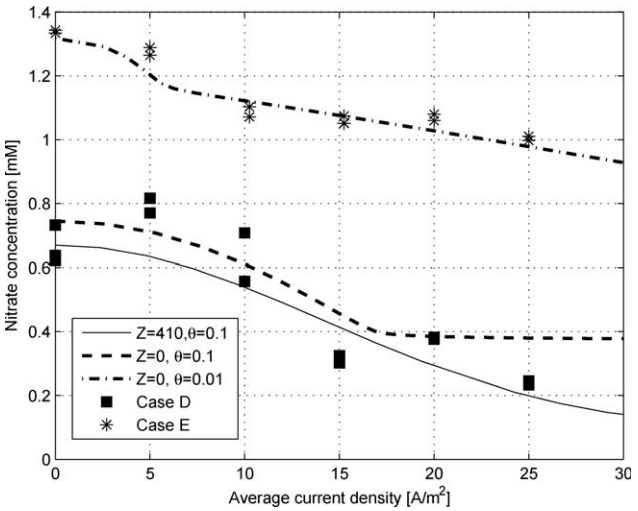

Figure 3. Nitrate concentration in the product water as a function of the applied current density.

Comparison between simulations with different textiles and the experimental results presented in a previous paper.[7]

The squares mark the nitrate concentration in the product obtained in the experiment with an ion-exchange textile incorporated in the FC. These results were presented as experimental case D in Ref. 7. In this experiment, the pressure in the concentrate compartment was increased to press the membranes against the textile to establish as good contact between textile and membrane as possible. Without current it was found that the incorporation of the textile into the FC led to an increased nitrate separation due to Donnan dialysis. This is believed to be due to an improved mixing of the liquid induced by the inherent structure of the network of fibers in the textile. When the current was applied, the nitrate level in the product decreased to levels which were well below the recommended maximum of 25 ppm. The squares in Figure 4 give the pH of the product. It was found that increasing the current density did not lead to the same dramatic change of the pH as was found in the case with a nonconductive textile. However, the pH of the product started to go down, indicating that water dissociation took place, when a current density of 25 A/m^2 was applied.

The values of the model parameters used in the simulations are presented in Table 1. The geometry of the cell and the flow rate used in the experiments were used to calculate the corresponding dimensionless parameter values. This will be the base case, which will be used to interpret the results

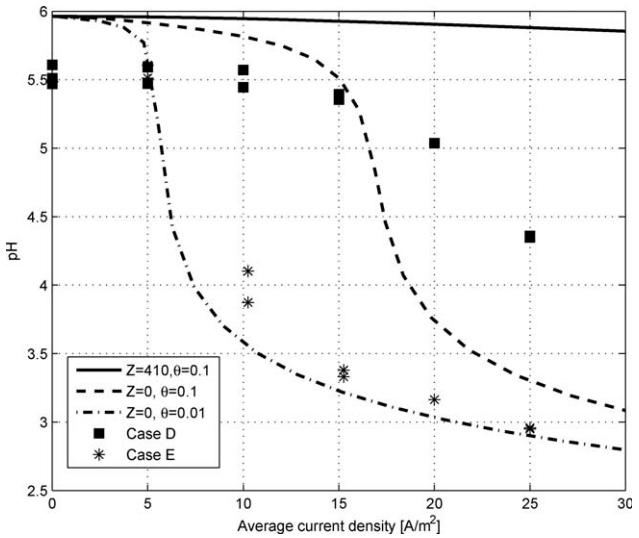

Figure 4. pH as a function of the applied current density.

Comparison between simulations with different textiles and experimental results presented in a previous paper.[8]

from the simulations. The values of the unknown parameters in the enhanced water dissociation model are chosen according to the estimates presented together with that model.[8] In this article, the diffusion coefficients of nitrate, chloride, and hydroxide in the membranes are taken to be 2% of their value in water, compared to 1.9% for chloride and 1.5% for nitrate, which was used in the simulations presented previously.[6,7,16] The estimates made for the quantities related to the ion-exchange textile were discussed in the experimental paper.[7] In the experiments, the CC were filled with a net-type spacer instead of an ion-exchange textile. However, the relatively high concentration of the solution in the CC makes the textile's influence on the results negligible.

During the experiments, only the cell voltage applied over the entire cell, the total current passed through the cell and the concentrations of the product and concentrate could be measured. This restricts the comparisons that can be made between model and experiments. Only the nitrate concentration and pH of the product as a function of the average current density applied can be compared.

The solid line in Figure 3 shows the nitrate concentration in the product as calculated with the model for the case where textile was incorporated. A good agreement is obtained with the experimental Case D. A comparison of the pH obtained in the experiments and simulations is presented in Figure 4. According to the simulations, the pH of the product should not change significantly when the current density is increased up to 30 A/m^2. Conversely, in the experiments a decrease of the product pH, down to 4.3, was found. This decrease of the pH indicates that water dissociation start to become important in this case also, which was not predicted by the model.

The dashed line in Figure 3 shows the result from a simulation with a textile with no functional groups incorporated, i.e., $Z = 0$. For low current densities, this simulation agrees well with the experimental points obtained with the conductive textile, i.e., Case D given by the squares in Figure 3. However, compared with the simulations with a conductive textile a higher χ value is required to obtain a specific current density. Thus, the use of a conductive textile reduces the power consumption. At about 17 A/m^2, the limiting current density is reached. A further increase of the current density implies water dissociation, which is also reflected in the pH of the product as shown in Figure 4. The pH is almost constant up to the point where the limiting current density is reached, whereas beyond this point the pH drops rather dramatically down to around three at 30 A/m^2.

Using a nonconductive textile seems very close to the experimental Case E where a nonconductive net-type spacer was used in the feed compartment. In the simulations with nonconductive textile, dashed line in Figures 3 and 4, far more nitrate was removed by Donnan dialysis, i.e., when the current density was not applied, compared with the experimental Case E. As discussed earlier, this can be explained by the good mixing induced by the fiber net-work of the textile. The limiting current density, indicated by the sudden drop in pH of the product, is for the same reason higher when the textile is used as a nonconductive spacer. Hence, also a textile without the ion-exchange groups will improve the efficiency of the process due to its mechanical structure, which will improve the mass transport in the feed compartment. A simulation where the coefficient of transversal dispersion was lowered by one order of magnitude, i.e., $\theta = 0.01$ gives a much better agreement with the experiments with the nonconductive net-type spacer, Case E; both the nitrate concentration and the pH curves are found to agree rather well. Thus, our model is capable of describing the water dissociation phenomenon in an electropermutation process with inert spacers relatively well. To make a better validation of the model, new experiments should be made with reference electrodes located in the center of the CCs. One could then compare the potential drop over the repeating unit with the response in both current density, pH and nitrate removal.

There are a number of possible explanations for the discrepancy between the prediction of the product pH made by the model and the experiments for the case where a conductive spacer was incorporated. Some of these will be discussed later.

Table 1. Values of the Nondimensional Parameters, Coefficients and Inlet Concentration used to Obtain the Results Presented in Figures 3 and 4

D_1	1.90[14]	Z	410
D_2	2.03[14]	C^{m}	1000
D_3	1.33[14]	α	0.10
D_4	5.26[14]	χ	0-0.66
D_5	9.31[14]	ε	0.15
D_0	$1 \cdot 10^{-9}$ [m^2 s^{-1}]		
c_{10} (FC)	1	κ	17
c_{30} (FC)	1	Λ	230
c_{40} (FC)	10^{-5}	θ	0.10
c_{50} (FC)	10^{-3}	Θ	0.07
c_{10} (CC)	6	Υ	0.03
c_{30} (CC)	120	$\hat{P}e$	380
c_{40} (CC)	10^{-5}	α_1^2	0.5
c_{50} (CC)	10^{-3}	α_1^4,α_1^{m2},α_1^{m4}	1
c_0	1.7 [mol m^{-3}][15]		

The model assumes a homogeneous textile, i.e., both the porosity and the distribution of the functional groups are assumed to be homogeneous. In the literature, several models for heat transfer to/from solid boundaries into porous beds introduce a variable porosity in the near wall region.[17,18] The variable porosity is then commonly described by an exponential function according.[18]

$$(1-\varepsilon) = (1-\varepsilon)_\infty \left(1 + b\exp\left(-\frac{c\xi}{d_f}\right)\right). \quad (43)$$

where b and c are empirical parameters, $(1\text{-}\varepsilon)_\infty$ is the void fraction in the bulk of the bed, and ξ is the coordinate in the wall normal direction. Not only does this effect the heat conduction in this region but it also gives a higher permeability close to the wall with a possible flow channeling in that region. In our case, where the fiber diameter is very small and the void fraction in the bulk is rather high the effect of flow channeling can be considered negligible. The effective mass transfer to the membrane is, however, affected. The value of the empirical parameter b is usually such that the void fraction at the wall is very close to unity. As a consequence of this the current density would be forced out into the liquid phase in a thin layer next to the membrane. The thickness of this layer is controlled by the other empirical parameter, c. Furthermore, the correlation for the mechanical dispersion used in the bulk is not likely to be valid all the way in to the membrane wall. This problem has been discussed in the literature and several different ways to model this has been proposed. A *van Driest* type of wall function was proposed by Cheng,[17–19]

$$\lambda = \lambda_\infty \left(1 - \exp\left(-\frac{m\xi}{d_f}\right)\right), \quad (44)$$

where λ_∞ is the transversal coefficient of dispersion in the bulk and m is an empirical parameter. Simulations have been carried out with both of these corrections included. However, using parameter values, which can be found in the literature, did not improve the pH predictions significantly. Thus, it is neither believed that the correlation used for the mechanical dispersion in the near wall region nor the assumption of a constant porosity should be responsible for the failure to accurately predict the pH drop with a conductive textile incorporated.

Another assumption made in the model is that the textile and the membrane are in perfect contact with each other. Ideally one would like the conductive spacer to be a porous continuation of the membrane with a very high specific area filling the whole feed compartment.[20] The situation in the experiments was that the textile spacer is made of a different material than the membrane and the fibers in the textile are not attached to the membrane surface. In the experiment, the pressure in the CC was higher than in the FC to force the membrane to be in contact with the textile. Even if this way of operating the process greatly improved the separation of nitrate and reduced the change of the pH, it does not mean that an ideal contact was established. It is very likely that some part of the membrane was not in direct contact with the membrane. Thus, it should be possible to improve the performance of the process by reducing the contact resistance between membrane and spacer. This contact resistance may be captured by the model used for the variable porosity, by tuning the parameters. This is, however, outside the scope of this article.

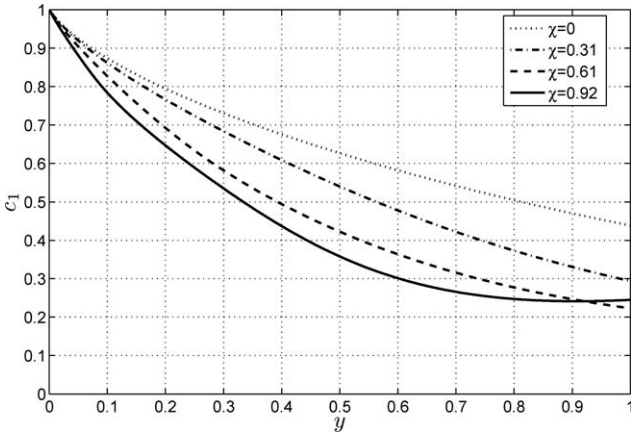

Figure 5. Nitrate concentration averaged over the F.C thickness as a function of streamwise coordinate.

Theses curves were calculated for an inert textile, $Z = 0$, other model parameters are according to Table 1.

Simulations with a nonconductive textile

The model will now be used to study the electropermutation process with a nonconductive textile, i.e., $Z = 0$, in more detail. The role of the textile in such a process would be to provide mechanical support to the ion-exchange membranes as well as improving the mixing of the liquid phase in the FC. Later, the capacity of the textile will gradually be increased to study the influence of a conductive spacer. In all these simulations, it will be assumed that the textile has a constant porosity and is in ideal contact with the membranes. Furthermore, the mechanical dispersion is assumed to be given by the same correlation used in the bulk all the way out to the membrane. Thus the model is more likely to underestimate the rate of water dissociation rather than overpredict it.

The concentration of nitrate averaged over the thickness of the FC as a function of the streamwise coordinate is shown in Figure 5. Each line represents simulations with a specific value of the nondimensional parameter χ, all other parameters are given in Table 1 except for Z which is set to zero. The dotted line, $\chi = 0$ represents the nitrate removal by Donnan dialysis. In this case, the nitrate level decreases steadily through the cell, which means that the whole compartment is active in the separation of nitrate. As the value of χ is increased, the rate of nitrate separation initially increases until the limiting current is reached. When the value of χ is increased above this point water dissociation becomes important. The partial current carried by OH^- in the membrane then increases rapidly when χ is further increased. For $\chi = 0.92$, which is the highest value presented in Figure 5, the nitrate removal is quite fast in the beginning of the cell. Then, as water starts to dissociate, the rate of nitrate removal decreases. In fact, the averaged nitrate

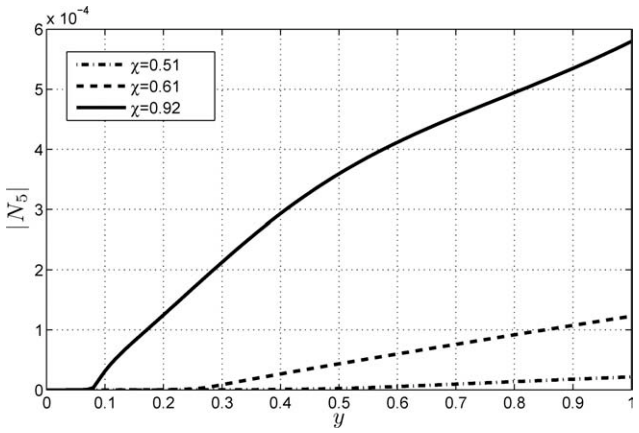

Figure 6. The flux of H^+ at $x = 1$.

This flux is given by the dissociation of water in the heterogeneous surface reaction.

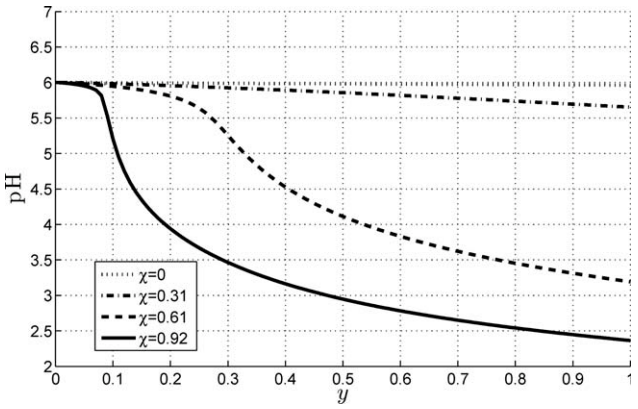

Figure 7. pH averaged over the F.C. thickness as a function of the stream wise coordinate.

Calculated with a nonconductive textile, $Z = 0$, and all other parameters as in Table 1.

concentration passes through a minimum and in the last section of the compartment more nitrate enters over the membrane on the cathode side than what leaves the FC over the membrane on the anode side. As a result, the nitrate level in the product actually is higher for $\chi = 0.92$ than for $\chi = 0.61$. Thus, the nitrate removal cannot be improved by increasing the applied potential further.

The membrane is assumed to be ideally selective so the flux of H^+ out from the membrane surface is that produced by the heterogeneous water dissociation. In Figure 6 the H^+ flux from the membrane surface is presented as a function of the streamwise coordinate for different values of χ. Close to the entrance of the FC the water dissociation is close to equilibrium. As one moves downstream through the FC the concentration boundary layer develops and the driving force for the enhanced water dissociation increases. The streamwise position for the onset of the enhanced water dissociation moves toward the inlet of the FC with increasing value of χ.

The pH of the liquid averaged over the F.C thickness is presented as a function of the vertical coordinate in Figure 7. For low values of χ, water dissociation is not significant and thus the pH stays roughly constant. Looking at the results from the simulations with the higher χ value, i.e., $\chi = 0.61$ and $\chi = 0.92$, it is clear that the significant water dissociation is taking place and the product pH goes down to 3.2 and 2.4, respectively. The vertical position where the enhanced water dissociation starts is clearly indicated in Figure 7 by the sudden pH drop. A reduced pH of the product also means that the pH in the CC is increased. High pH close to the membrane in the concentrate compartment may be a serious problem for the reliability of the process. Most metal hydroxides have a low solubility and if the OH^- concentration becomes too high precipitation of salts such as iron hydroxides can foul the membrane.[21]

The total ionic concentration of the water in the FC increases when water begins to dissociate. This will lead to an increased conductivity of the liquid, which will influence the current distribution. In Figure 8, the current density scaled with the current density at the inlet is shown as a function of streamwise coordinate for different values of χ. When the applied potential is very low, the current density is almost constant all the way through the cell. Then, if the applied potential drop is increased, but not enough for water dissociation to become important, one finds that the current density is highest in the beginning of the FC and then gradually decreases as one moves through the cell. As nitrate ions in the feed are replaced by slightly more mobile chloride ions, this decrease of the current density cannot be explained by the change in the composition of the feed water. A more likely explanation would be that concentration polarization taking place close to the membranes leads to an increased resistance of the cell. If the potential is further increased, water dissociation will eventually start to become important. This will increase the total salinity of the water in the FC by producing highly mobile H^+ ions that remain in the FC. A consequence of this is that the conductivity of the FC increases, which is seen by the increase in current density as

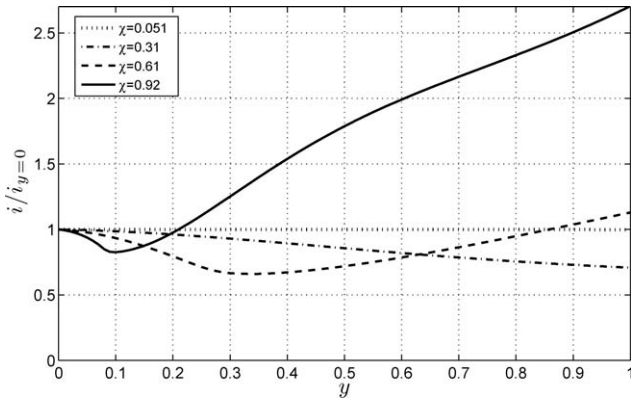

Figure 8. The current density distribution, scaled by the current density at the inlet, through the cell as predicted by the model in a simulation for a nonconductive textile, i.e. $Z = 0$.

All other parameters as given in Table 1.

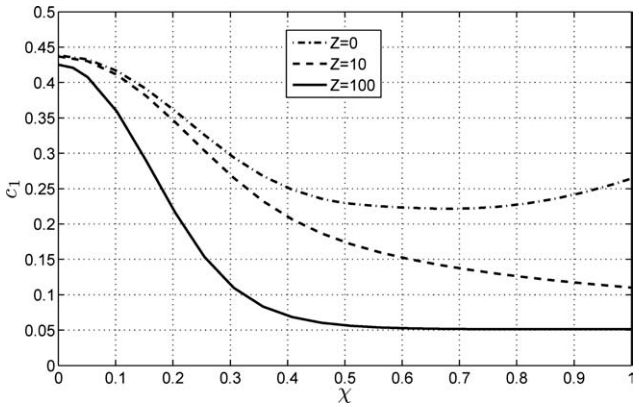

Figure 9. Nitrate concentration in the product as a function of the dimensionless parameter χ.

Each line corresponds to a different textile capacity.

one moves downstream through the cell. Thus at $\chi = 0.92$, the highest current density close to the outlet is almost three times higher than at the inlet. At the same time the nitrate removal is very poor in the region close to the outlet.

To summarize, simulations with a nonconductive textile were performed to gain some insight into this simplified process. The maximum nitrate separation possible to accomplish was found to be just under 75%, with the chosen set of parameter values. In the base case studied in this paper where the initial nitrate level is 105 ppm this gives that the lowest nitrate level that could be obtained is that which is the recommended maximum level, i.e. 25 ppm. However, the pH of the product in this case would be about 3 which is very low, and the local pH next to the membrane in the CC would be as high as 11 close to the outlet. Furthermore, it is likely so that if the flow rate or the thickness of the FC is increased, in order to increase the productivity per unit membrane area, the nitrate level of maximum 25 ppm in the product cannot be reached. Thus, to increase the productivity a conductive spacer has to be used.

Simulations with a conductive textile

To study the influence of a conductive textile in the FC, simulations were performed with different textile capacities. The parameter values used in the simulations are given in Table 1 except for the scaled textile capacity Z, which was varied.

In Figure 9, the nitrate level in the product is presented as a function of χ for three different values of Z. The dash-dotted line represents a simulation with a nonconductive textile, $Z = 0$. As discussed earlier, the nitrate concentration of the product passes through a minimum as the value of χ is increased. This minimum is located between $\chi \approx 0.55 - 0.75$ in the simulations presented here. If instead a textile with a very low capacity, $Z = 10$, is used; the nitrate level decreases with increasing χ all the way up to $\chi = 1$. The nitrate concentration in the product at $\chi = 1$ is just above 10% of the feed water concentration. Hence, a feed water with around 100 ppm of nitrate could be treated, and a level under the recommended level of max 25 ppm nitrate[22,23] could be reached using this textile.

The solid line in Figure 9 represents results from simulations with $Z = 100$, i.e., a textile with higher capacity. It is clear that the nitrate separation is very fast with this textile. At $\chi \approx 0.5$ the limit of the separation possible to achieve is reached. As was concluded in our previous paper,[6] an increased textile capacity makes the optimal value of χ decrease in such a way that the product between the optimal χ value and Z is constant.

The current density passed through the cell at a given value of χ is dependent on the capacity of the textile. In Figure 10, polarization curves for three different textile capacities, $Z = 0$, 10, and 100, are presented. The polarization curve obtained with a nonconductive textile, represented by the dash-dotted line, shows three different regions. First the current density increases linearly with χ up to $\chi \approx 0.3$. The region, $0.3 \lesssim \chi \lesssim 0.5$, shows a plateau due to the limiting current denity. In the third and final region the current density again rises with increasing χ. This super limiting current density is in our simulations a result of the enhanced water dissociation. Because of the dissociation of water, the conductivity of the liquid in the FC increases. As a consequence of this, the current density, obtained in our simulations with a nonconductive textile, is higher than when a conductive textile, $Z = 100$, is used at $\chi = 10$.

The dashed line represents the polarization curve obtained in a simulation with a textile with poor conductivity, $Z = 10$. In this case, the most of the current is passed through the liquid phase. Thus, the initial slope of the polarization curve is very close to the case with a nonconductive textile. When the concentration close to the membrane approaches zero, the conductivity of this phase becomes very low and the current moves into the fiber phase in this region. This reduces the sharp increase of the electric field in the liquid phase next to the membrane. The current density in the liquid phase close to the membrane surface is kept low and hence the dissociation of water is suppressed. Thus, the partial current of H^+ and OH^- remains low even for rather high χ values. This explains why the conductive textiles reduce the water dissociation intensity.

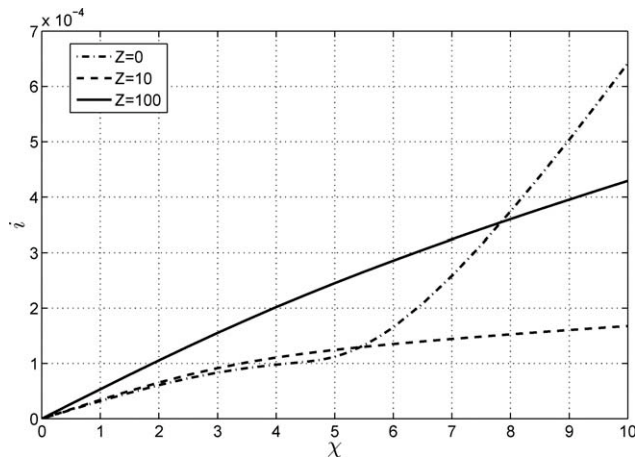

Figure 10. Current density as function of χ, i.e., polarization curves, for different Z values.

The polarization curve for the textile with $Z = 100$ is represented by the solid line in Figure 10. In this case, the fiber phase has a reasonable conductivity. Both phases carry half of the current each in the bulk of the FC. This makes the total conductivity of the FC higher compared with the case with an inert textile. Hence, the initial slope of the polarization curve is higher. As the concentration in the liquid phase becomes low, the current moves into the fiber phase instead and the limiting current behavior is not seen. Compared with the case when the textile had a relatively poor conductivity the resistance close to the membrane in the fiber phase is lower and the slope of the polarization curve is therefore higher.

In both cases, when a conductive textile was used the enhanced water dissociation was suppressed. Thus, most of the current is carried through the membrane by NO_3^- and Cl^- for all values of the current density. As a consequence of this no minimum for the nitrate separation for $\chi \leq 1$ could be found. In Figure 11, the flux of nitrate at the membrane, x=1, in simulations with $\chi = 0.51$ is presented as a function of streamwise position, y. The dash-dotted line is obtained in a simulation with $Z = 0$. In this case, the total nitrate flux is passed through the liquid phase. The solid and dashed lines represent the nitrate fluxes in the fiber and liquid phases, respectively, in a simulation with $Z = 100$. The nitrate flux in the fiber phase is rather high close to the inlet of the cell, where most nitrate is replaced by chloride. This also explains the low nitrate fluxes in the last part of the cell.

As pointed out earlier, the pH of the product should be considered when finding suitable operating conditions for the process. Also the local pH in CC next to the membrane should be taken into account. In Figure 12 the pH, averaged over the thickness of the F.C, as a function of streamwise coordinate in a simulation with $Z = 100$ and $\chi = 0.36$ is given by the solid line. The dashed line represents the local pH next to the membrane in the CC, i.e., $x = 1+\Theta$. It is found that the pH of the product decreases only slightly from pH 6 down to 5.7, which can be acceptable. The pH next to the membrane in the C.C reaches a value of about 8.5 close to the outlet of the cell. This value is not very high and can be acceptable. If, however, this pH should increase to higher values there might be problems with fouling of the membrane due to precipitation of hydroxides.

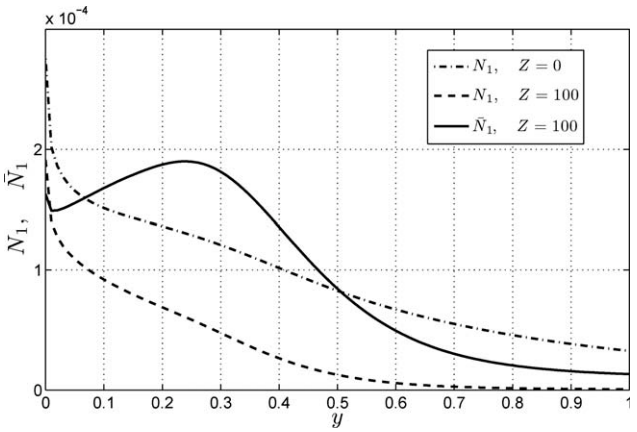

Figure 11. Nitrate flux in the different phases at the membrane surface $x = 1$, for two different capacities of the textile and $\chi = 0.51$.

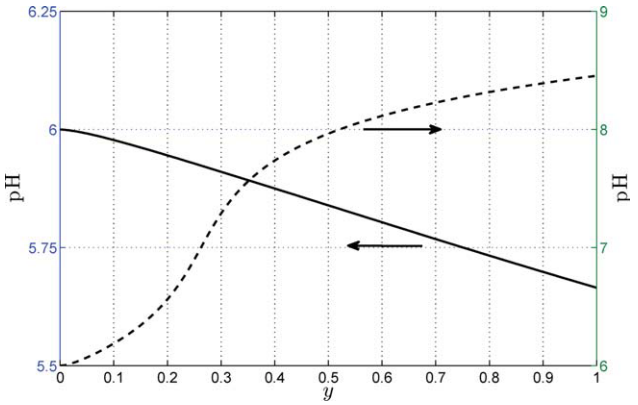

Figure 12. The solid line represents the pH (scale on the left *y*-axis) averaged over the thickness of the feed compartment, obtained in a simulation with $Z = 100$ and $\chi = 0.36$.

The dashed line is the local pH (scale on the right y axis) next to the membrane in the concentrate compartment. [Color figure can be viewed in the online issue, which is available at wileyonlinelibrary.com.]

Conclusion

The model for the enhanced water dissociation at surfaces of ion-exchange materials was successfully implemented in the simulations of nitrate removal by continuous electropermutation. For the case where a net-type spacer was used the model could predict pH variations in the product that were in line with the experimental observations previously reported. Thus, it was concluded that the new model is a powerful tool that can be used to study electromembrane processes.

Simulations with a nonconductive textile highlighted the limitations of such a process configuration. The separation of nitrate, possible to accomplish, is limited by concentration polarization taking place close to the surface of the membrane. Increasing the current density above the limiting current density gives rise to an enhanced water dissociation, which leads to a change of the pH of the product water. Furthermore, the pH in the CC might lead to fouling problems due to precipitation of hydroxide salts. In the base case considered in this article, the minimum nitrate level that could be reached in the product when a nonconductive textile was used was 25 ppm. However, the pH would then be as low as three in the product and as high as 11 close to the membrane in the concentrate compartment. Thus, the productivity has to be lowered if a nonconductive textile is used.

To investigate the influence of the capacity of the ion-exchange textile, simulations were performed with two different capacities of the fiber phase. It was found that using these textiles the dissociation of water was reduced considerably. The optimal χ value is reduced when Z is increased in such a way that the product χZ remains constant. Thus, a higher Z value reduces the power consumption of the process by reducing the resistance of the feed compartment. As

the concentration of the liquid phase approaches zero close to the membrane, due to the concentration polarization, the current density moves into the fiber phase. Concentration polarization does not take place in the fiber phase due to the fixed counter ions. Thus, the limitation for the nitrate flux is moved from the surface of the ion-exchange membrane to the much larger surface of the fiber phase.

Simulations indicated that incorporation of an anion-conductive textile in the FC of the electropermutation equipment reduces the water dissociation tendency. It is believed that an insufficient contact between the textile and the membranes in the experiments can explain the relatively poor prediction of the pH. Poor contact increases the power consumption of the process as well as the risk of enhanced water dissociation. The dissociation of water is an unwanted phenomenon in the process studied in this article. First of all it will decrease the current efficiency of the process. Furthermore, it will lead to pH changes of the product water, but perhaps even more disturbing is the increase of the pH next to the membrane in the concentrate compartment, which may cause fouling of the membrane as previously discussed.

The first step for improving the process would be to solve the problems related to the poor contact between the membrane and the textile. If this can be accomplished, the separation method appears very attractive with existing ion-exchange textiles and membranes.

Notation

c = nondimensional concentration in liquid phase
$\bar{c}$ = nondimensional concentration in fiber phase
$\tilde{\bar{c}}$ = concentration in fiber phase [mol m^{-3}]
$\tilde{c}^{\mathrm{m}}$ = concentration in membrane [mol m^{-3}]
$\tilde{c}$ = concentration [mol m^{-3}]
c_0 = concentration scale [mol m^{-3}]
c_{i0} = nondimensional inlet concentration
c_0^{m} = concentration of mobile ions in membrane [mol m^{-3}]
$c_{\mathrm{H_2O}}$ = concentration of water in water [mol m^{-3}]
C^{m} = concentration ratio $\frac{c_0^{\mathrm{m}}}{c_0}$
C^{w} = concentration ratio $\frac{\sqrt{K_{\mathrm{w}}}}{c_0}$
d_{f} = average fibre diameter [m]
D_0 = typical diffusion coefficient [m^2 s^{-1}]
D_{T} = coefficient of transversal dispersion [m^2 s^{-1}]
j = nondimensional flow velocity
$\tilde{j}$ = flow velocity [m s^{-1}]
j_0 = characteristic flow velocity [m s^{-1}]
K = permeability [m^2]
K_{w} = Ionic product of water [mol^2 m^{-6}]
k_{b} = reaction rate of water recombination in bulk [mol m^{-3} s^{-1}]
k_{b}^0 = surface reaction rate [mol m^{-2} s^{-1}]
k_{f} = reaction rate of waterdissociation in bulk [s^{-1}]
L = vertical height [m]
$\tilde{N}$ = flux density in liquid phase [mol m^{-2} s^{-1}]
$\tilde{\bar{N}}$ = flux density in fibre phase [mol m^{-2} s^{-1}]
N = nondimensional flux density in liquid phase
$\bar{N}$ = nondimensional flux density in fibre phase
P = pressure [Pa]
$\hat{P}e$ = nondimensional parameter $\frac{h}{L}\frac{j_0 h}{D_0}$
$\mathcal{R}$ = nondimensional surface reation rate
$\tilde{S}$ = reaction rate [mol m^{-3} s^{-1}]
S = nondimensional reaction rate
$\mathcal{V}$ = nondimensional cell voltage
w = concentration of mobile ions in fibre phase [mol m^{-3}]
x = nondimensional horizontal coordinate
$\tilde{x}$ = dimensional horizontal coordinate[m]
y = nondimensional vertical coordinate
$\tilde{y}$ = dimensional vertical coordinate [m]
z_i = valence of specie i
Z = concentration ratio $\frac{w}{c_0}$

Subscripts

1 = NO_3^-
2 = Cl^-
3 = Na^+
4 = OH^-
5 = H^+

Greek letters

α = model coefficient
α_i^j = ion-exchange equilibrium coefficient in textile
α_i^{mj} = ion-exchange equilibrium coefficient in membrane
ε = volume fraction of fibre phase
Θ = ratio between membrane thickness and FC width
θ = nondimensional parameter $\frac{\lambda d_{\mathrm{f}} L}{h^2}$
κ = nondimensional reaction rate constant
Λ = nondimensional parameter $\sqrt{\frac{(1-\varepsilon)}{K}}h$
λ = constant in the expression for the transversal dispersion coefficient
μ = dynamic viscosity [Pa s]
Υ = nondimensional surface reaction rate
ξ = coordinate in wall normal direction [m]
$\tilde{\phi}$ = potential in liquid phase [V]
ϕ = nondimensional potential in liquid phase
$\tilde{\bar{\phi}}$ = potential in fibre phase [V]
$\bar{\phi}$ = nondimensional potential in fibre phase
χ = nondimensional parameter $\frac{\mathcal{V}}{\hat{P}e}$

Literature Cited

1. Helfferich F. *Ion Exchange*. Dover, 1995. ISBN 0–486-68784–8.
2. Ganzi G, Egozy Y, Giuffrida A, Jha A. Deionization-high purity water by electrodeionization performance of the ionpure continuous deionization system. *Ultrapure Water*. 1987;4:43–48.
3. Ganzi GC, Jha AD, DiMascio F, Wood JH. Electrodeionization theory and practice of continuous electrodeionization. *Ultrapure Water*. 1997;14:64–68.
4. Ezzahar S, Cherif A, Sandeaux J, Sandeaux R, Gavach C. Continuous electropermutation with ion-exchange textiles. *Desalination*. 1996;104:227–233.
5. Smara A, Delimi R, Poinsignon C, Sandeaux J. Electroextraction of heavy metals from dilute solutions by a process combining ion-exchange resins and membranes. *Sep Purif Technol*. 2005;44:271–277.
6. Danielsson CO, Dahlkild A, Velin A, Behm M. Nitrate removal by Continuous electropermutation using ion-exchange textile. I. Modeling. *J Electrochem Soc*. 2006;153:D51–D61.
7. Danielsson CO, Velin A, Behm M, Dahlkild A. Nitrate removal by continuous electropermutation using ion-exchange textile. II. Experimental investigation. *J Electrochem Soc*. 2006;153:D62–D67.
8. Danielsson CO, Dahlkild A, Behm M, Velin A. A Model for The enhanced water dissociation on monopolar membranes. *Electrochim Acta*. 2009;54:2983–2991.
9. Whitaker S. *The Method of Volume Averaging*. Kluwer Academic Publisher, 1999. ISBN 0–7923-5486–9.
10. Bear J. *Dynamics of Fluids in Porous Media*. Dover, 1988. ISBN 0–486-65675–6.
11. Clague DS, Kandhai BD, Zhang R, Sloot PMA. Hydraulic permeability of (un)bounded fibrous media using lattice Boltzmann method. *Phys Rev E*. 2000;61:616–625.
12. Koponen A, Kandhai D, Hellén E, Hoekstra A, Kataja M, Niskanen K, Sloot P, Timonen J. Permeablility of three-dimensional random fiber webs. *Phys Rev Lett*. 1998;80:716–719.
13. Greenkorn R. *Flow Phenomena in Porous Media*. Dekker, 1983.
14. Newman JS. *Electrochemical Systems*. 2nd ed. Prentice Hall, 1991.
15. Passounaud M, Bollinger J, Serpaud B, Lacour S. Water nitrate removal with ion-exchanger grafted textiles. *Environ Technol*. 2000; 21:745–753.

16. Elattar A, Elmidaoui A, Pismenskaia N, Gavach C, Pourcelly G. Comparison of transport properties of monovalent anions through anion-exchange membranes. *J Membr Sci*. 1998;143:249–261.
17. Kaviany M. *Principles of Heat Transfer in Porous Media*, 2nd ed. Springer, 1999.
18. Cheng P. Fully developed forced convective flow through an annular packed-sphere bed with wall effects. *Int J Heat Mass Transfer*. 1986;29:1843–1853.
19. Hsu CT, Cheng P. Thermal dispersion on a porous medium. *Int J Heat Mass Transfer*. 1990;33:1587–1597.
20. Rubinstein I, Oren Y, Zaltzman B. Multi-phase model of a sparse ion-exchange spcer. *J Membr Sci*. 2004;239:3–8.
21. Strathmann H. *Ion-Exchange Membrane Separation Processes*. Elsevier, 2004.
22. European Union. Council directive of 3 November 1998. *Off J Europ Commun*. 1998;L330:0032–0054.
23. WHO. *Guidlines for Drinking Water Quality; Recomendations I*, 3rd ed. Geneva: WHO, 2004.

Manuscript received Apr. 23, 2009, revision received Aug. 31, 2009, and final revision received Nov. 16, 2009.